PLOS ONE

Interaction Studies of the Human and *Arabidopsis thaliana* Med25-ACID Proteins with the Herpes Simplex Virus VP16- and Plant-Specific Dreb2a Transcription Factors

Ximena Aguilar[1], Jeanette Blomberg[2], Kristoffer Brännström[2], Anders Olofsson[2], Jürgen Schleucher[2], Stefan Björklund[2]*

1 Department of Chemistry, Umeå University, Umeå, Sweden, 2 Department of Medical Biochemistry and Biophysics, Umeå University, Umeå, Sweden

Abstract

Mediator is an evolutionary conserved multi-protein complex present in all eukaryotes. It functions as a transcriptional co-regulator by conveying signals from activators and repressors to the RNA polymerase II transcription machinery. The *Arabidopsis thaliana* Med25 (aMed25) ACtivation Interaction Domain (ACID) interacts with the Dreb2a activator which is involved in plant stress response pathways, while Human Med25-ACID (hMed25) interacts with the herpes simplex virus VP16 activator. Despite low sequence similarity, hMed25-ACID also interacts with the plant-specific Dreb2a transcriptional activator protein. We have used GST pull-down-, surface plasmon resonance-, isothermal titration calorimetry and NMR chemical shift experiments to characterize interactions between Dreb2a and VP16, with the hMed25 and aMed25-ACIDs. We found that VP16 interacts with aMed25-ACID with similar affinity as with hMed25-ACID and that the binding surface on aMed25-ACID overlaps with the binding site for Dreb2a. We also show that the Dreb2a interaction region in hMed25-ACID overlaps with the earlier reported VP16 binding site. In addition, we show that hMed25-ACID/Dreb2a and aMed25-ACID/Dreb2a display similar binding affinities but different binding energetics. Our results therefore indicate that interaction between transcriptional regulators and their target proteins in Mediator are less dependent on the primary sequences in the interaction domains but that these domains fold into similar structures upon interaction.

Introduction

Mediator is a multi-protein transcriptional co-regulator complex which is conserved in eukaryotes [1–3]. It acts as a bridge by transmitting signals from promoter-bound transcription regulators (activators and repressors) to the general RNA polymerase II (Pol II) machinery to regulate transcription of protein encoding genes [4,5], but its function at the molecular level is still elusive. Mediator is structurally dynamic and has a high conformational flexibility which depends on intrinsically disordered regions within some of its protein subunits [6,7]. These regions are prone to fold upon interaction with transcriptional regulators which induces structural changes in Mediator required for propagation of regulatory signals to the Pol II transcription machinery [8–10]. Mediator is evolutionary conserved from yeast to humans but individual Mediator subunits have diverged and some of them share only modest sequence homologies between different organisms [1,2,11]. In addition, the number of Mediator subunits differs between organisms, from 25 in yeast to 29 and 34 in humans and plants, respectively. The higher number of subunits in higher eukaryotes is likely related to the increased complexity of transcription regulation in multicellular organisms [2,12–15].

Med25 is one of the few Mediator subunits that are specific to higher eukaryotes and human Med25 (hMed25) has been shown to interact with several transcription factors involved in different cellular processes, including retinoid signaling by RARα, chondrogenesis by SOX9, insulin secretion in pancreatic cells by HNF4α, cellular growth and differentiation by PEA3 subfamily members and endoplasmic reticulum stress response by ATF6α [16–19]. A specific ACtivator Interaction Domain (ACID) in hMed25 has been shown to interact with the Herpes simplex virus type 1 VP16 protein and the Varicella-zoster virus protein IE62, which activate transcription of viral genes [20–23]. The structure of the hMed25-ACID (residues 394–543) has been solved by NMR and it comprises seven β-strands forming a β-barrel flanked by three helices [24,25]. The interaction between hMed25-ACID and VP16 has been studied in detailed and the VP16 binding site in the ACID has been defined [20,22]. In addition to binding to the hMed25-ACID, the VP16 transcription activation domain (TAD) has been shown to interact with several general transcription factors, including TFIIA, TFIIB, TFIIF, TFIIH, TBP, hTAF$_{II}$31/hTAF$_{II}$32 (Taf9), Med15 and Med17 to activate immediate early genes during lytic infection [20,26–34]. The VP16-TAD is composed of two subdomains, one N-terminal

including residues 412–452 and one C-terminal which includes residues 452–490, which function independently and complementary [22,31,35,36]. Similar to several other TADs (*e.g.* p53), the VP16-TAD is unstructured in its free, unbound state, but adopts an α-helical conformation upon binding to its target proteins [30,40]. Within the two subdomains, the formation of α-helical segments has been located to residues 429–450 and 465–488 [37]. In the N-terminal TAD, a nine-amino acid sequence (DFDLDMLGD) has been identified as playing a key role for VP16 transcription activity [35,41]. In addition, this nine-amino acid motif has also been identified in several other transcription factors and it is proposed to bind to a common co-factor. This is the case for VP16, p53, HSF1, NF-kB and NFAT1, which all contain this motif and have been shown to interact with the TAF$_{II}$31 (TAF9) protein [42].

The *A.thaliana* Med25 (aMed25) was originally identified as *PHYTOCHROME AND FLOWERING TIME 1* (*PFT1*), which function in a phyB pathway to regulate the expression of the *FLOWERING LOCUS T* (*FT*) in response to suboptimal light conditions [43–45]. More recently, *PFT1* was identified as Med25 and has been shown to be involved in regulation of jasmonate (JA) signaling and different stress response pathways [12,46,47]. Med25 interaction with specific transcription factors results in both positive and negative regulatory effects. MYC2 interaction with Med25 is involved in activation of JA-responsive gene expression; while Med25 interaction with ABI5 had a negative regulatory effect on regulation of Abscisic acid mediated gene expression, [48]. We have previously shown that the aMed25-ACID interacts with three transcription factors; the Dehydration responsive element binding protein 2A (Dreb2a), the Myb-like transcription factor and the zinc finger homeodomain 1 protein [46]. Dreb2a interacts with cis-acting dehydration-responsive promoter elements and activates genes involved in drought- and salt stress responses [49,50]. The transcription activation domain of Dreb2a has been localized to residues 254–335 [51] but the minimal domain required for interaction with aMed25-ACID in yeast 2-hybrid assays was localized to residues 168–254 [46] and is thus distinct from the Dreb2a TAD. The target for the Dreb2a activation domain is therefore likely to be another, yet not identified Mediator subunit. In a previous study we found that a fragment of Dreb2a (residues 168–335; Dreb2a$_{168-335}$), which includes both the TAD and the Med25 interaction domain is unstructured in the free state and was required to bind aMed25-ACID with a high affinity *in vitro* [52]. In the same study we also showed that hMed25-ACID was able to interact with Dreb2a, which is remarkable in two aspects. First, the ACIDs from *A.thaliana* and human share low sequence similarity (16%) and secondly, Dreb2a is a plant-specific transcription factor belonging to the large AP2/ERBP (ethylene responsive element binding protein) transcription factor family [53–55].

In the present study we use GST pull downs- and surface plasmon resonance (SPR) experiments to show that the VP16-TAD interacts with the aMed25-ACID. Furthermore, using NMR chemical shift perturbation (CSP) and isothermal titration calorimetry (ITC) combined with available information about the well-studied interaction between hMed25-ACID and VP16-TAD, we show that the two unrelated transcription factors Dreb2a and VP16 interact with overlapping regions in the ACIDs of both human and plant Med25. Our results suggest that the Med25-ACIDs from human and *A.thaliana* retain a conserved structure and function regarding activator binding, despite a low level of homology in primary sequence. This highlights the importance of studying cross-species interactions between transcriptional regulators and their target proteins.

Results

aMed25-ACID interacts with the Herpes Simplex virus VP16 transcription factor

Previous studies have shown that hMed25-ACID interacts with the VP16-TAD [24,25,36,56] and we have previously reported that hMed25-ACID unexpectedly interacts with the plant-specific Dreb2a transcription factor, even though hMed25-ACID and aMED25 show very low sequence homology. In order to study if also aMED25-ACID and VP16 can interact, we carried out binding experiments between the aMed25-ACID and the VP16-TAD using pull-downs and SPR. In our experiments we used two constructs of the GST-VP16-TAD protein to test the binding properties of the different VP16 subdomains. One construct contained the N-terminal functional subdomain (TADn) comprising residues 412–452. The second construct (VP16-TAD) contained both subdomains (residues 427–485; **Figure 1A**). GST pull-down experiments were carried out with the aMed25-ACID, but also with the hMed25-ACID as a positive control (**Figures 1B and 1C**). Western blotting using antibodies against GST and aMed25-ACID revealed binding of aMed25-ACID with both VP16-TAD-constructs (**Figure 1B**). Next, we tested if the interaction between aMed25-ACID and the VP16 TADs could be inhibited by the *A.thaliana* transcription factor Dreb2a, which we have previously shown to interact with the aMed25-ACID [46,52]. For these pull-down experiments we used a 6 x his-tagged, C-terminally extended domain of Dreb2a, which comprised both the aMed25-binding domain (BD; 168–253) and the activation domain (AD; 254–335) (**Figure 1A**). We carried out the binding reactions as described above, but this time aMed25-ACID and Dreb2a$_{168-335}$ were pre-incubated together before they were added to GST-VP16-TADs pre-bound to glutathione beads. Proteins bound to the beads were identified by Western blotting using anti-GST and anti-Med25 antibodies. As shown in **Figure 1D**, aMed25-ACID did not bind to the VP16-TADn when it had been pre-incubated with Dreb2a$_{168-335}$. Similar results were obtained when using VP16-TAD (data not shown). The finding that Dreb2a$_{168-335}$ interferes with the binding of aMed25-ACID to the VP16-TAD indicates that both Dreb2a and VP16 interact with overlapping regions on the aMed25-ACID.

The interactions between different Med25-ACID and VP16-TAD proteins were further analyzed using SPR. The GST-VP16-TAD and GST-VP16-TADn subdomains were immobilized on a CM5 sensor chip using amine coupling and binding was assessed for both the hMed25-ACID (as positive control) and the aMed25-ACID. The sensogram profiles were similar for all four interactions, displaying both rapid association and dissociation kinetics. The binding kinetics was obtained by monitoring sensograms with increasing concentrations of Med25-ACID proteins injected to the immobilized VP16-TAD subdomains (**Figure 2A–F**). The dissociation constants (K_D) were calculated to 2.4 µM and 1.8 µM for the aMed25-ACID/VP16-TADn and the aMed25-ACID/VP16-TAD interactions, respectively. The K_D values obtained for the hMed25-ACID/VP16-TADn (5.4 µM) and the hMed25-ACID/VP16-TAD (2.8 µM) interactions were in the similar range. Furthermore, the K_D value for interaction between the hMed25-ACID and the VP16-TADn that we obtained in our experiments is comparable to those previously reported (1.6 µM) by Wagner et al., using ITC [56].

NMR-studies of interactions between Dreb2a and hMed25-ACID or aMed25-ACID

We have previously shown that both hMed25-ACID and aMed25-ACID interact with the *A.thaliana* Dreb2a transcription
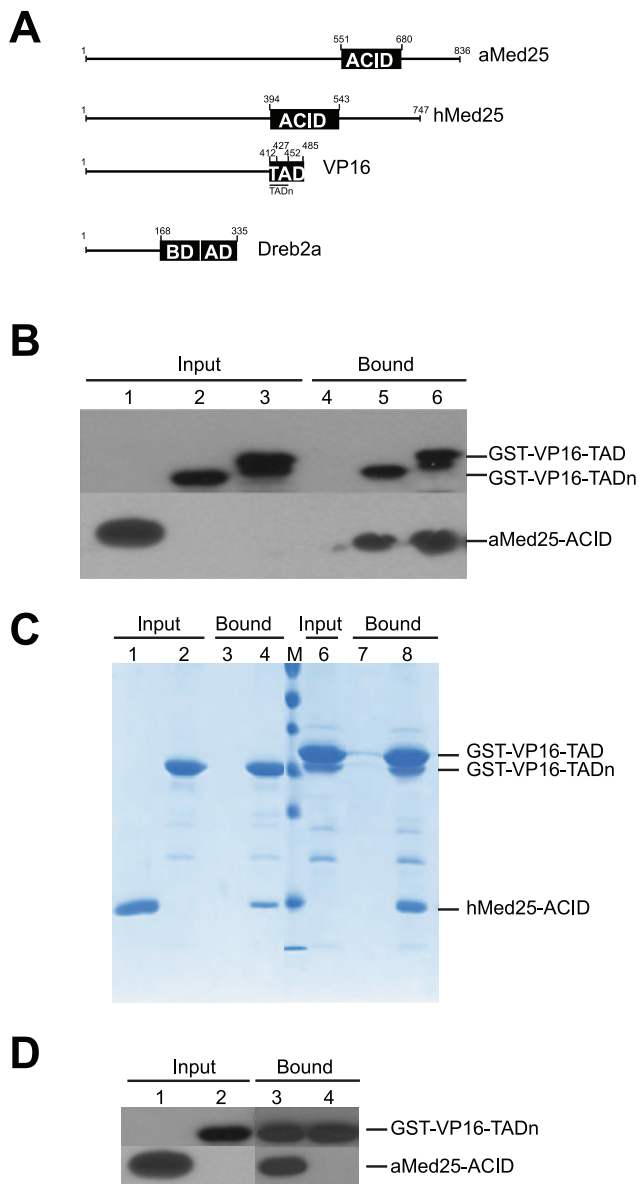
Figure 1. *A.thaliana* and human Med25-ACIDs interacts with the Herpes Simplex virus VP16 transcription factor. A) Illustration of the protein domains used in this study. ACID, activator interaction domain. TAD and AD, transcription activation domains. BD, *A.thaliana* Med25-ACID-binding domain. **B)** GST pull-down assay using purified recombinant proteins. aMed25-ACID was incubated with glutathione beads pre-bound to GST-VP16-TADs and the proteins were visualized by immunoblotting with anti-GST and anti-Med25 antibodies. Lane 1, aMed25-ACID (input); Lane 2, GST-VP16-TADn (input); Lane 3, GST-VP16-TAD (input). Lane: 4, aMed25-ACID (bound); Lane 5, aMed25-ACID + GST-VP16-TADn; Lane 6, aMed25-ACID + GST-VP16-TAD (bound). The input lanes represent 25% of the load used for each pull-down experiment. **C)** GST pull-down assay using recombinant proteins. GST-VP16-TADs were pre-bound to glutathione beads and incubated with hMed25-ACID (18 kDa). Proteins were separated on a 15% SDS-PAGE and stained with Coomassie blue. Lane 1, hMed25-ACID (input); Lane 2, GST-VP16-TADn (input); Lane 3, hMed25-ACID (bound); Lane 4, hMed25-ACID + GST-VP16-TADn (bound); Lane 6, GST-VP16-TAD (input); Lane 7, hMed25-ACID(bound); Lane 8, hMed25-ACID + GST-VP16-TAD (bound). **D)** GST pull-down assay to study competition between binding of Dreb2a$_{168-335}$ and VP16-TAD to aMed25-ACID. Dreb2a$_{168-335}$ and aMed25 were pre-incubated and then added to VP16-TADn bound to GST-beads. Lane 1, aMed25-ACID (input); Lane 2, GST-VP16-TADn (input); Lane 3, aMed25-ACID + GST-VP16-TADn

(bound), Lane 4, aMed25-ACID pre-incubated with Dreb2a$_{168-335}$ + GST-VP16-TADn (bound). The input lanes represent 25% of the load used for each pull-down experiment.

factor [52]. Since the hMed25 ACID structure is known and its binding site for VP16-TAD is defined [24,36,56], we performed NMR CSP experiments in order to map the Dreb2a binding site(s) in hMed25 and to explore if the hMed25-ACID binding interface(s) for VP16-TAD and Dreb2a overlaps. NMR titration experiments were performed using isotope-labelled ^{15}N hMed25-ACID and unlabeled Dreb2a$_{168-335}$. A series of two-dimensional (2D) ^{1}H,-^{15}N heteronuclear single quantum-coherence (HSQC) spectra was recorded using ^{15}N-labeled hMed25-ACID in free form and in the presence of different concentrations of Dreb2a$_{168-335}$ (molar ratios of hMed25-ACID:Dreb2a$_{168-335}$: 1:0.2; 1:0.4; 1:0.6; 1:1; 1:2). Chemical shift assignments of hMed25-ACID were obtained from the Biological Magnetic Resonance Data Bank (BMRB, ID 17139). The chemical shift changes were analyzed at the 1:1 ratio because the affected peaks were either undetectable or showed curved chemical shift changes in the ^{1}H, ^{15}N plane at higher concentrations of Dreb2a$_{168-335}$ (**Figure 3A**, inset). The changes in the chemical shifts of the amide resonances of hMed25 upon binding to Dreb2a$_{168-335}$ (1:1 ratio) were plotted against the residue number in **Figure 3B** where the positions of the seven β-strands and three α-helices that comprise hMed25-ACID are indicated. An adjusted chemical shift value ($\Delta\delta$) was calculated according to $\Delta\delta = [(\Delta\delta H)^2 + (0.2\Delta\delta N)^2]^{1/2}$ in order to weight contributions of ^{1}H and ^{15}N [57]. A threshold value was set based on two times the standard deviation σ ($2\sigma = 0.10$) [58]. Residues that displayed major chemical shifts ($\Delta\delta > 0.10$ ppm) in the ^{1}H,-^{15}N HSQC spectra were T424, S426, Q451, Q456, L458, C497, H499, T503, I521, L525 and G536. The largest effects observed were located to strands β3 and β5, which along with the other five β-strands form a β-barrel which contains a hydrophobic pocket (**Figure 3C**).

During the CSP experiments we observed several interesting features. First, we found that the hMed25-ACID residues that underwent chemical shift changes upon addition of Dreb2a were in the fast- and intermediate exchange range on the NMR time scale. In the fast exchange range, peaks did not change significantly in intensity and the shifts occurred continuously during the titration. In the intermediate exchange range (the majority of the chemical shifts above 0.10 belong to this category) the intensity of the peaks decreased and showed line-broadening while the chemical shifts changed from an unbound to a bound state (**Figure 3A**, inset). Second, ~35% of the peaks disappeared already at the first titration ratio (1:0.2) (**Figure 3A, D**), indicating that they are directly or indirectly involved in the binding event. However, the disappearance of these NH at this low molar ratio of Dreb2a$_{168-335}$ indicates that they are in an intermediate exchange regime. This prevented us from obtaining information about these residues, although they might be important for complex formation, because we were unable to add Dreb2a$_{168-335}$ at high enough concentrations due to problems with its solubility and stability. Third, we noticed that some cross-peaks had a tendency to shift in a curved-like manner (**Figure 3A** inset) which might result from secondary binding effects. Such secondary binding effects might include weak or non-specific binding of Dreb2a$_{168-335}$ on additional sites on hMed25-ACID, or formation of higher-order complexes. It is likely that these effects are caused by the activation domain of Dreb2a, which is unstructured and potentially forms transient structural segments upon interaction with hMed25-ACID, a feature that has previously been reported for transcrip-
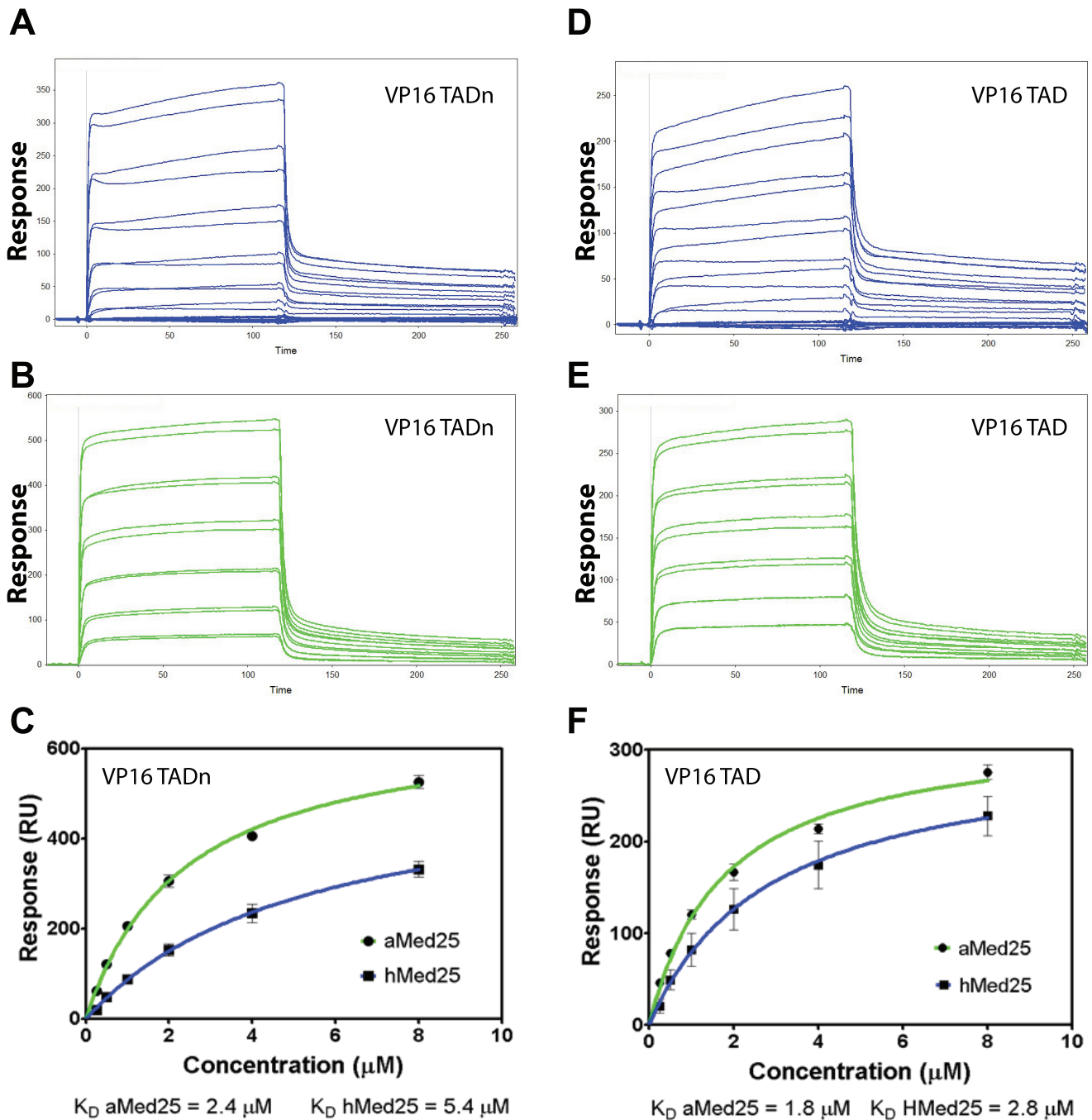
Figure 2. Binding kinetics for VP16-TADn and VP16-TAD to *A.thaliana* and human Med25-ACIDs. A) SPR sensogram for association and dissociation of hMed25 to GST-VP16-TADn. **B**) SPR sensogram for association and dissociation of aMed25 to GST-VP16-TADn. **C**) Binding curves plotted from the sensograms in A and B. The dissociation constants (K_D) are indicated. **D**) SPR sensograms for association and dissociation of hMed25 to GST-VP16-TAD. **E**) SPR sensograms for association and dissociation of aMed25 to GST-VP16-TAD. **F**) Binding curves plotted from the sensograms in D and E. The dissociation constants (K_D) are indicated. Green curves represent aMed25 and blue curves represent hMed25.
doi:10.1371/journal.pone.0098575.g002

tional activators upon interaction with its targets [39,59–61]. For example the VP16-TAD forms helical segments upon interaction with Tfb1, PC4 and hTAF$_{II}$31 [30,37,38,60]. Such potential helical segments can also be predicted to form in Dreb2a (**Figure S1**). Finally, we mapped the significant chemical shifts and the residues that were undetectable already at the first titration point onto a ribbon diagram of the hMed25 NMR structure (PDB ID 2XNF) [36] (**Figure 3C**). From this diagram we can observe that

the β-barrel that forms the hydrophobic pocket in hMED25-ACID is the most affected during ligand titration. This hydrophobic pocket has previously been described to play an important role in the hMed25-ACID/VP16-TAD interaction [56]. Interestingly, some residues that display significant chemical perturbations in our titration experiments (T424, Q451, Q456, L458, C497, H499, L525) have been described to constitute part of the interaction surface with VP16-TAD [24,36,56]. Q451 has been
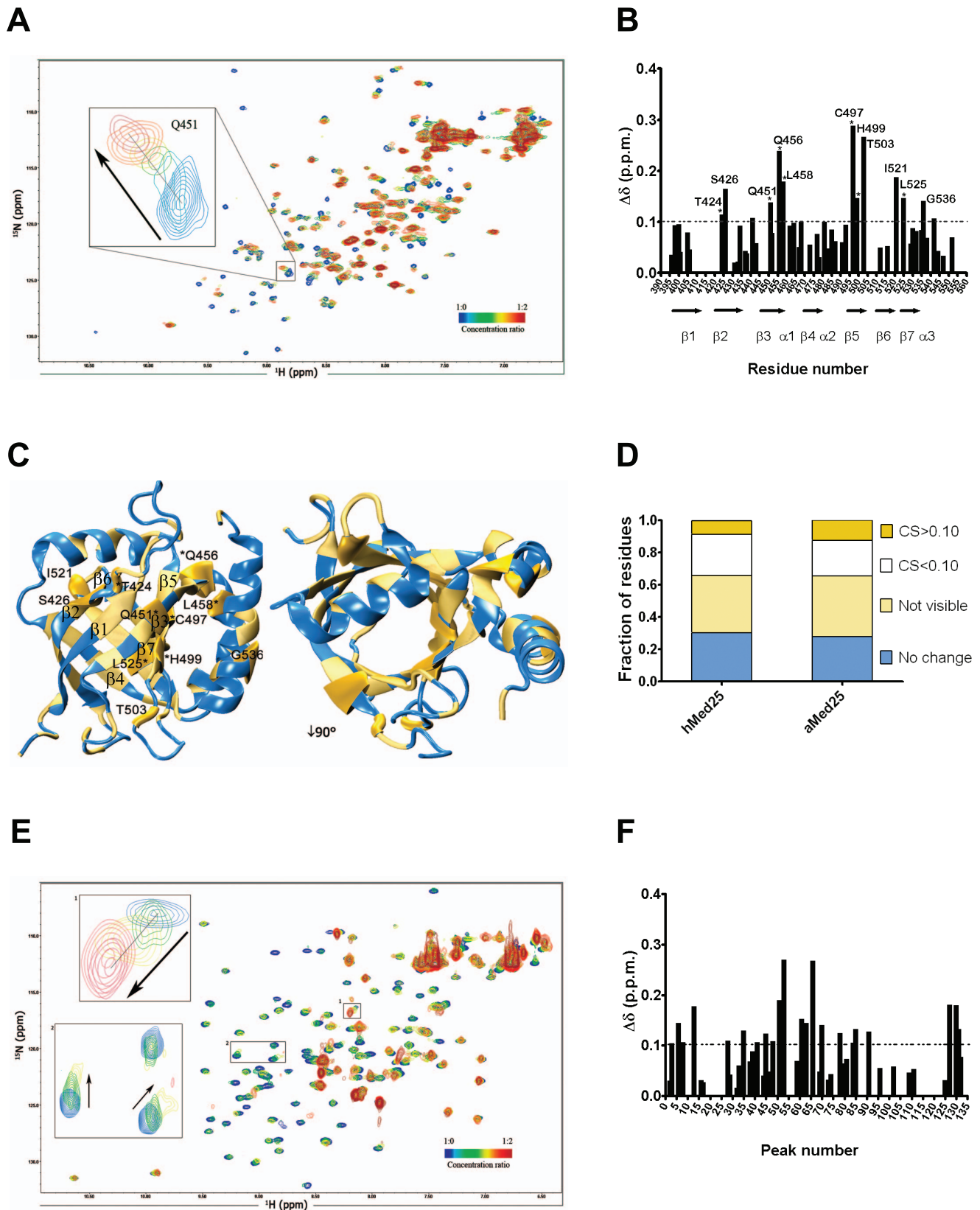
Figure 3. NMR studies of interactions between Dreb2a and hMed25-ACID or aMed25-ACID. A) ^{1}H,-^{15}N HSQC spectra of hMed25-ACID in the absence (blue) and in presence of 0.2 (cyan), 0.4 (green), 0.6 (yellow), 1 (orange) or 2 equivalents (red) of Dreb2a$_{168-335}$. Inset shows an intermediate exchange shift of a resonance corresponding to residue Q451 with a curved-like shift. **B**) Chemical shift changes ($\Delta\delta$) obtained from NMR experiments shown in (A) plotted against the residue number of hMed25-ACID. The position of the seven β-strands and three α-helices is

indicated under the residue numbers. Residues undergoing major chemical shift changes ($\Delta\delta > 0.10$ ppm) are labeled with the respective residue number and asterisks indicate residues which have been previously reported to be part of the interaction surface with VP16-TAD [36,56]. Dotted line corresponds to the threshold value of 0.10 (two chemical shift standard deviations). **C**) NMR structure of hMed25-ACID (PDB ID 2XNF) [36]. Residues undergoing significant chemical shifts upon addition of Dreb2a$_{168-335}$ from figure (B) are enlarged and highlighted in gold and labeled with residue name and number. Resonances which are broadened beyond detection by interaction with Dreb2a$_{168-335}$ are colored in light yellow. The seven β-strands are indicated in the left view. **D**) Comparison of the fraction of peaks which are affected to differing degrees by interaction of Dreb2a$_{168-335}$ with Med25-ACID proteins, based on spectra presented in figure 3A and 3E. Color coding indicates peaks which are unaffected (blue), broadened beyond detection (light yellow), $\Delta\delta > 0.1$ (gold), $\Delta\delta < 0.1$ (white). **E**) ^{1}H,-^{15}N HSQC spectra of aMed25-ACID in the absence (blue) and in presence of 0.2 (green), 0.5 (yellow), 1 (orange) or 2 equivalents (red) of Dreb2a$_{168-335}$. Inset 1 shows a cross-peak illustrating fast exchange with a curved-like shift. Inset 2 shows fast exchange shifts of two resonances (indicated by arrows). **F**) Similar plot as (B) but using data obtained from NMR experiments showed in (E). $\Delta\delta$ was plotted against the number of peaks corresponding to the number of residues of aMed25-ACID. No peak assignment is available for aMed25-ACID, therefore an identification of residues undergoing significant chemical shift changes is not possible.
doi:10.1371/journal.pone.0098575.g003

reported to have a critical role for the interaction with VP16-TADn since a mutation of Q451 to a glutamic acid prevents binding [56]. Moreover, as in the case for the hMed25-ACID/VP16-TAD interaction described by other studies [36,56], we also observed that a large interaction surface centered on the inside or core of the β-barrel in the hMed25-ACID is affected upon binding to Dreb2a (**Figure 3C**). In summary, our results suggest that the ligand binding interface(s) in hMed25-ACID that participate in interactions with VP16-TAD and Dreb2a$_{168-335}$ are similar or overlapping, and that the formation of hMed25-ACID/VP16-TAD and hMed25-ACID/Dreb2a$_{168-335}$ complexes give rise to similar conformational rearrangements.

Similar NMR CSP experiments were performed using ^{15}N-labeled aMed25-ACID together with unlabeled Dreb2a$_{168-335}$ or full-length Dreb2a (Dreb2a$_{f.l.}$). 2D ^{1}H,-^{15}N HSQC spectra of aMed25-ACID were recorded in free form and in the presence of different molar ratios of aMed25-ACID and Dreb2a$_{f.l.}$ (aMed25-ACID: Dreb2a$_{f.l.}$; 1:0.2; 1:0.5; 1:1; 1:2). In this titration, a majority of the NMR signals disappeared with increasing concentrations of Dreb2a (**Figure S2**). Due to this fast transition, the rate at which the components of the complex exchanged between the free and bound state was difficult to analyze. Some signals shifted and decreased in intensity (**Figure S2**, inset 1), indicating fast exchange. Other signals decreased in intensity without shifting, most likely due to strong line broadening in the intermediate exchange regime (**Figure S2**, inset 2). In theory, broadened signals should reappear if the equilibrium can be shifted fully towards the complex. However, we were unable to observe such new signals because the fraction of complex remained small due to the problems with solubility and stability, which made it impossible to use Dreb2a$_{f.l.}$ at higher concentrations.

In the NMR titration using Dreb2a$_{168-335}$ (19 kDa) we also observed that several resonances were strongly affected (loss of intensity) by the addition of Dreb2a$_{168-335}$ at the 1:1 ratio (**Figure 3E**). However, the number of detectable NMR signals of aMed25-ACID was higher compared to the titration using the Dreb2a$_{f.l.}$ protein. During the titration experiment, we observed shifts of some aMed25-ACID resonances upon addition of increasing concentrations of Dreb2a$_{168-335}$. These chemical shifts correspond to an intermediate and fast exchange (**Figure 3E,** inset 1,2) and some of them showed similar curved-like types of shifts (**Figure 3E,** inset 1) reminiscent of to those observed in the hMed25-ACID/Dreb2a$_{168-335}$ titration experiment (**Figure 3A**). The structure of aMed25-ACID has not been solved, which makes it difficult to map the interaction site(s) precisely. However, by plotting the chemical shifts difference ($\Delta\delta$) for all aMed25-ACID amide groups (**Figure 3F**), we found that the number of significant shifts was comparable to those obtained in the hMed25-ACID/Dreb2a$_{168-335}$ experiment (compare **Figures 3B and 3F**). In addition, by comparing the amount of unaffected and undetectable residues upon titration with increasing amount of

Dreb2a with the results from the hMed25-ACID experiment, we observed a similar behavior for both hMed25-ACID and aMed25-ACID (**Figure 3D**). This comparison suggests that hMed25-ACID and aMed25-ACID undergo similar conformational changes upon interaction with Dreb2a$_{168-335}$. Based on the secondary structure prediction for aMed25-ACID (**Figure S3**), which indicates a similar content of secondary elements as the hMed25-ACID, and our results showing that hMed25-ACID and aMed25-ACID behave in a comparable manner upon interaction with Dreb2a, we speculate that the ACID domains from human and *A.thaliana* Med25 display a similar interaction surface which can adopt a similar structure upon interaction with Dreb2a.

Complex formation of Med25-ACID proteins and Dreb2a studied by ITC

To obtain further insights into the binding mechanisms between hMed25-ACID and aMed25-ACID with Dreb2a, we preformed ITC experiments. 20 μM Med25-ACID and 200 μM Dreb2a$_{168-335}$ were used for these titrations. The calorimetry data was evaluated using the standard model of bimolecular complex formation for single-site binding. We obtained thermodynamic data from the binding curve-fittings as shown in Table 1. Based on the obtained affinity constants (K_A), the K_D values were calculated to 5.4 μM and 3.0 μM for the hMed25-ACID/Dreb2a$_{168-335}$ and the aMed25-ACID/Dreb2a$_{168-335}$ interactions, respectively. The binding free energy values obtained for both the hMed25-ACID/Dreb2a$_{168-335}$ and aMed25-ACID/Dreb2a$_{168-335}$ interactions, were small (-7 kcal/mol), which is characteristic for weak and transient protein-protein interactions, such as those typically observed between transcriptional regulators and their target proteins [62]. Even though the binding affinities and free energies that we observed for complex formation were similar to each other (**Figure 4A, B**), the binding mechanisms differed based on the large difference between the enthalpic and entropic contributions from the formation of each of the complexes (**Figure 4C, Table 1**). The comparison between the binding energetics from the two different interaction events showed large differences; the aMed25-ACID/Dreb2a$_{168-335}$ interaction was more enthalpy-driven compared to the hMed25-ACID/Dreb2a$_{168-335}$ interaction (**Figure 4C**). The negative enthalpy change, which originates from favorable weak interactions at the protein-protein surface (i.e. hydrogen- and van der Waals bonds) was almost 2-fold larger for the aMed25-ACID/Dreb2a$_{168-335}$ interaction compared to the hMed25-ACID/Dreb2a$_{168-335}$ interaction. In addition, the unfavorable change in entropy, which may be caused by folding of Dreb2a$_{168-335}$ into a more well-defined structure upon complex formation, was around 4-fold larger for aMed25-ACID/Dreb2a$_{168-335}$ compared to the corresponding values for the hMed25-ACID/Dreb2a$_{168-335}$ interaction (**Figure 4C**). These results suggest that the complex formation between Dreb2a$_{168-335}$ and aMed25-ACID involves larger conformational rearrange-
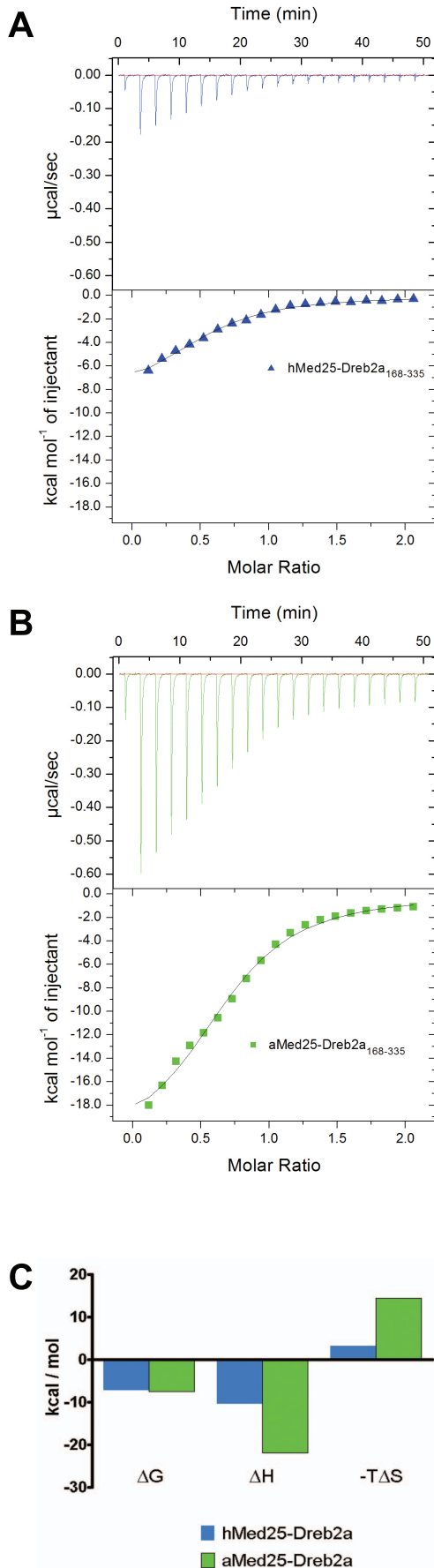
Figure 4. Complex formation of Med25 and Dreb2a studied by ITC. A) ITC profile corresponding to the binding of hMed25-ACID/Dreb2a$_{168-335}$ (blue, triangles). **B**) ITC profile corresponding to the binding of aMed25-ACID/Dreb2a$_{168-335}$ (green, squares). 200 µM Dreb2a$_{168-335}$ (in the syringe) was titrated into 20 µM hMed25-ACID (A) or 20 µM aMed25-ACID (B) in the reaction chamber at 25°C. The plots in the lower panels in A and B are integrated heats from raw data (upper panels) as a function of the molar ratio of Dreb2a/Med25-ACID. The binding curves were fitted using a single site binding model (Origin, MicroCal). The thermodynamic data obtained from the fitting are presented in figure (C) and Table 1. **C**) Histograms of the binding energetics from the two binding events in (A and B) showing the differences in enthalpic and entropic contributions from each complex formation. hMed25-ACID/Dreb2a$_{168-335}$ (blue) and aMed25-ACID/Dreb2a$_{168-335}$ (green). Change in free binding energy (ΔG), change in binding enthalpy (ΔH) and change in entropy factor (ΔTS).
doi:10.1371/journal.pone.0098575.g004

ments compared to those that occur upon binding between hMed25-ACID and Dreb2a$_{168-335}$.

From our NMR results on these interactions, we deduced that binding of Dreb2a$_{168-335}$ affects large regions in both of the Med25-ACID proteins. However, we could not directly describe the different binding mechanisms that were deduced from our ITC experiments. Similar unfavorable entropy changes were obtained in a study between the transcriptional coactivator β-Catenin and the unstructured transcription factor Lef-1 [63]. The process of binding between two or more proteins -which confers functionality-, is the result of several complementary attributes at the protein's interfaces, ranging from the amino acid composition, hydrophobicity, electrostatic interactions and hydrogen bonding. All these attributes determine the energetics of the protein-interfaces and the free energy contributions have to be kept in balance for stable complex formation. This process involves a balance between entropy and enthalpy changes where the unfavorable changes might be compensated in the regions that are not part of the binding site [64–67], which might explain the differences in binding energetics between hMed25-ACID/Dreb2a and aMed25-ACID/Dreb2a. Therefore, even though the plant-specific transcription factor Dreb2a is able to bind to the hMed25-ACID, it might still give rise to a different and specific functional fold upon complex-formation with the aMed25-ACID which might be required for proper functionality during activation of transcription in *A.thaliana*. Similar ITC experiments using VP16 were not carried out since GST cleavage of the fusion protein resulted in very low yields wherefore the protein concentrations required for performing ITC experiments could not be obtained.

Discussion

We have used a series of protein-protein interaction methods to show and characterize the binding between Med25-ACID from human and *A.thaliana*, with the Herpes simplex virus VP16- and plant specific Dreb2a transcription factors. Several studies have already described the interaction between hMed25-ACID and VP16-TAD, and the binding site has been mapped [24,36,56]. To our knowledge, this is the first time that human herpes simplex virus VP16-TAD has been reported to interact with *A.thaliana* Med25-ACID. Our earlier findings showing that hMed25-ACID interacts with the *A.thaliana* transcription factor Dreb2a [52], were here studied in more detail using NMR and ITC. Our NMR experiments showed that the hMed25-ACID interaction surface for Dreb2a$_{168-335}$ overlaps partially with the previously reported VP16-TAD binding site [24,36,56]. VP16 and Dreb2a are unrelated transcription factors that display an amino acid sequence identity of only 11% (**Figure S1**). Notably, we found

Table 1. Thermodynamic data extracted from ITC measurements.

	ΔG (kcal/mol)	ΔH (kcal/mol)	$T\Delta S$ (kcal/mol)	K_A (M^{-1})	K_D (μM)
hMed25-Dreb2a	−7.18	−10.43	−3.24	1.84E5	5.4
aMed25-Dreb2a	−7.50	−21.94	−14.43	3.28E5	3.0

Binding parameters were determined by using a single site binding model (Origin, MicroCal). Total free binding energy change ΔG, enthalpy change ΔH, entropy factor change ΔTS, affinity constant K_A and dissociation constant K_D.
doi:10.1371/journal.pone.0098575.t001

that six amino acids in the Dreb2a sequence are identical and aligns to a region in VP16-TAD containing nine amino-acids (DFDLDMLGD), which has previously been reported as important for interaction with several regulatory proteins [41,68]. This nine amino-acid sequence has also been identified in a range of transcription factors and might represent a novel motif which can be recognized by a common co-factor. Such is the case for VP16, p53, HSF1, NF-kB and NFAT1 which both contain the nine amino-acid sequence and interact with the general co-activator TAF9 (TAFII31) [30,42,69]. However, this motif is absent in the two other transcription factors, Myb-like and ZFHD1, which we identified as interacting with Med25-ACID in the same two-hybrid screen were we found Dreb2a [46]. This is not surprising, since we found that ZFHD1 and Myb-like are involved in stress-response pathways, while Dreb2a in addition is involved in regulation of light-quality pathways downstream of the PhyB receptor.

On the other hand, the human and *A.thaliana* Med25-ACID homologs share only 16% identity in amino acid sequence but their secondary structure contents appear to be highly similar (**Figure S3**). Despite the low homology, our study shows that the ACIDs from each of the human and *A.thaliana* Med25 are able to interact with both of the unrelated transcription regulators VP16 and Dreb2a *in vitro*. In addition, both transcription regulators seem to share interaction surfaces on the Med25-ACIDs. It is likely that both the transcriptional regulators and the Med25-ACIDs contribute to the recognition specificity for these particular protein-protein interactions. At one side, the VP16 and Dreb2a TADs both belong to the acidic activator family and share the nine amino-acid common motif found in several other TADs. On the other side, the ACIDs from human and *A.thaliana* show structural similarities which might provide the interaction surfaces required for binding of the transcriptional regulators. Moreover, our study provides insight into the mechanism for interaction between Dreb2a and the Med25-ACID proteins. Our NMR experiments show that a comparable fraction of both arabidopsis and human Med25-ACID residues are affected upon binding of Dreb2a. A detailed analysis of the interaction surfaces is hampered by strong line broadening probably due to secondary binding effects. These effects influence our NMR results, but are not detected in our ITC or SPR experiments, because of the higher protein concentrations used in the NMR experiments. Our ITC data indicate that the proteins have similar affinities but different binding energetics, which might result in distinct conformational rearrangements upon complex formation. The conformational changes appear to be larger for the interaction between the Med25-ACID and Dreb2a$_{168-335}$ from *A.thaliana* relative to the human Med25-ACID and Dreb2a$_{168-335}$. This might be relevant for proper biological function in the normal context, where the Mediator complex in *A.thaliana* needs to be triggered by interaction with Dreb2a to induce the structural rearrangements that are required to perform its function. As mentioned in the introduction, Mediator has been

shown to be structurally dynamic and flexible and the binding to activators induces global structural shifts [9].Our ITC experiments showed differences in energetics when comparing Dreb2a binding to human or *A.thaliana* Med25-ACIDs. We therefore speculate that the plant transcription factor Dreb2a might not induce such structural shifts upon interaction with human Med25-ACID since these proteins originate from different species. It would be interesting to compare these results with the conformational changes that VP16-TAD would induce in *A.thaliana* Med25-ACID. However, as already mentioned such experiments could not be performed due to difficulties to achieve sufficiently high protein concentrations. Altogether, our findings that the ACID from human and plant Med25 can interact with the unrelated VP16 and Dreb2a transcription factors, suggest that even though the Mediator complex sequences have diverged rapidly during evolution, the structure and interaction properties of its subunits remain conserved.

Materials and Methods

Protein expression and purification

Full-length 6 x his-GB1 tagged Dreb2a (Dreb2a$_{f.l.}$), 6 x his-tagged Dreb2a$_{168-335}$, *A.thaliana* Med25$_{551-680}$ (aMed25-ACID) and 6 x his-tagged human Med25$_{394-543}$ (hMed25-ACID) were expressed in *E. coli* BL21 pLysS cells and purified as described previously [46,52]. Cells for expression of isotope labeled human and *A.thaliana* Med25-ACID were grown in M9 medium (22 mM Na$_2$HPO$_4$, 22 mM KH$_2$PO$_4$, 8.5 mM NaCl, 22.2 mM glucose, 1 mM MgSO$_4$, 0.1 mM CaCl$_2$, 29.6 μM thiamine, 40.9 μM biotin and trace elements, pH 7.4) containing 18.6 mM ^{15}NH$_4$Cl as the only nitrogen source. Expression was induced by addition of isopropyl β-D-1-thiogalactopyranoside (IPTG) to a final concentration of 0.5 mM at an OD$_{600}$ of 1. The cells were then grown over night at 18°C and proteins were purified as described [52]. pETM30 vectors encoding VP16-TAD constructs (TADn: residues 412–452; VP16-TAD: residues 427-485) were kindly provided by Prof. Gerhard Wagner (Harvard Medical School, BCMP). The vectors were transfected into *E. coli* BL21 pLysS and protein expression was induced by addition of IPTG to a final concentration of 1 mM at an OD$_{600}$ of 0.8 followed by incubation for four hours at 30°C. GST-fusion VP16-TAD proteins were purified by affinity chromatography on glutathione-sepharose 4B (GE Healthcare) following the manufacturer's instructions. All purified proteins were transferred in to buffer A (20 mM Tris/HCl pH 7.5, 150 mM Na$_2$SO$_4$, 0.5 mM DTT) using dialysis cassettes or spin columns (Thermo Scientific). Protein samples were concentrated using ultrafiltration spin columns (Vivaspin, Sartorius) and the protein concentrations were calculated by determining their absorption at 280 nm and by using the proteins' extinction coefficients (E$_{280}$ M^{-1} cm^{-1}: 15,470 for aMed25-ACID, 22,460 for hMed25-ACID, 66,350 for Dreb2a$_{f.l.}$, 26,930 Dreb2a$_{168-335}$, 44,350 for GST-VP16-TAD and 42,860 for GST-

VP16-TADn). The protein concentration for VP16-TADn, which lacks tyrosines and tryptophanes, was calculated based only on the extinction coefficient for GST ($E_{280} = 42,860 \text{ M}^{-1} \text{ cm}^{-1}$).

GST pull-down experiments

For each reaction, 5 μM GST-VP16-TAD were bound to 20 μl glutathione-sepharose beads which had been pre-washed in an equilibration buffer (20 mM Tris/HCl pH 7.5, 150 mM Na_2SO_4) for one hour at 4°C. The beads were washed with equilibration buffer and pre-bound GST-VP16-TAD proteins were incubated with 5 μM of human Med25 or *A.thaliana* Med25 at 4°C. For the competition assays, 5 μM each of the *A.thaliana* Med25-ACID and 5 μM $Dreb2a_{168-335}$ proteins were pre-incubated for 1 hour at 4°C. Unbound proteins were collected in the flow-through and proteins bound to the beads were washed three times with 1 ml of ice-cold equilibration buffer. Bound proteins were the directly eluted by boiling in sample buffer. 2.5% of the bound proteins from each reaction were separated on 15% SDS-PAGE and proteins were identified by Western blotting using anti-GST (Sigma) and anti-aMed25-ACID (Agrisera) antibodies.

Surface Plasmon Resonance

The SPR experiments were performed using a Biacore 3000 instrument (GE Healthcare). GST-VP16-TADs were immobilized onto a CM5 sensor chip by amine coupling according to the manufacturer's instructions (GE Healthcare). About 500 resonance units (RU) of GST-VP16-TADs were immobilized using 10 mM sodium acetate buffer pH 4.5 and HBS-EP as running buffer (10 mM HEPES pH 7.4, 150 mM NaCl, 3 mM EDTA). Kinetics experiments were carried out by injecting decreasing concentrations of hMed25-ACID and aMed25-ACID (8 μM with 2-fold dilutions down to 0.25 μM) at a flow rate of 20 μl/min (running buffer: 20 mM Tris/HCl pH 7.5, 150 mM Na_2SO_4). Experiments were performed in duplicates and data was analyzed using the Scrubber2 (BioLogic software) and illustrated using the Graph Pad software.

NMR chemical shift perturbations experiments

NMR titration experiments were performed on a Bruker Avance III 850 MHz spectrometer equipped with a $^{-1}$H, ^{13}C, ^{15}N TCI cryoprobe. 2D HSQC spectra were recorded for ^{15}N-labeled hMed25-ACID or ^{15}N-labeled aMed25-ACID (150 μM) in the absence and in the presence of increasing concentrations of unlabeled $Dreb2a_{168-335}$ (molar ratio hMed25-ACID:$Dreb2a_{168-335}$: 1:0.2; 1:0.4; 1:0.6; 1:1; 1:2) (molar ratio aMed25-ACID:$Dreb2a_{168-335}$: 1:0.2; 1:0.5; 1:1; 1:2). For the NMR titration with $Dreb2a_{f.l.}$, 2D HSQC spectra of 25 μM ^{15}N-labeled aMed25-ACID were recorded in its free state and in the presence of 12.5, 25 and 50 μM $Dreb2a_{f.l.}$. The sample for each titration point was prepared independently and used at these low concentrations since $Dreb2a_{f.l.}$ precipitates at higher concentrations. All experiments were recorded at 25°C in 20 mM Tris/HCl pH 7.5, 150 mM Na_2SO_4, 0.5 mM DTT, 10% (v/v) D_2O. Data were processed using Topspin 3.0 software (Bruker) and analyzed using the NMRviewJ software. Assignments of backbone chemical shifts of human Med25-ACID were obtained from the Biological magnetic Resonance bank with the accession number 17139 (www.bmrb. wisc.edu). Chemical shift changes of ^{1}H and of ^{15}N were weighted using the formula $\Delta\delta = [(\Delta\delta H)^2 + (0.2\Delta\delta N)^2]^{1/2}$ [57] to take the chemical shift ranges of ^{1}H and ^{15}N into account.

Isothermal titration calorimetry

Binding experiments were performed using an auto ITC_{200} (MicroCal, GE Healthcare) at 25°C. Protein concentrations in the reaction chamber were 20 μM of hMed25-ACID or 20 μM of aMed25-ACID. 200 μM $Dreb2a_{168-335}$ was used in the syringe for the titration. For the control experiment, Dreb2a was titrated into buffer A (20 mM Tris/HCl pH 7.5, 150 mM Na_2SO_4, 0.5 mM DTT). For each experiment, we performed 19 automated injections of 2 μl each with 150 s intervals between each injection and with a stirring speed of 1000 rpm. The titrations were repeated twice. Calorimetric data were plotted and fitted using the standard single-site binding model (Origin, MicroCal).

Supporting Information

Figure S1   Sequence alignment of the TADs from Dreb2a and VP16. Asterisks indicate identical amino acids. The regions in VP16-TAD which have propensity to form α-helices upon interaction with its target are indicated (435–450 and 465–485) [37]. The black box indicates the region of the nine-amino-acid sequence that has previously been reported as important for interaction of VP16-TAD with several co- factors [41,66] and which also has been identified in a range of transcription factors such as VP16, p53, HSF1, NF-kB and NFAT1 [30,42,67]. The Dreb2a sequence has six identical amino acids that align to that region in VP16-TAD (DFDLDMLGD).
(EPS)

Figure S2   Interaction between aMed25-ACID and Dreb2a$_{f.l.}$. 2D ^{1}H,-^{15}N HSQC spectra of aMed25-ACID in the absence (blue) and in the presence of 0.2 (green), 0.5 (yellow), 1 (orange) and 2 equivalents (red) of $Dreb_{f.l.}$. Fast transition between the free and bound state could not been analyzed. Inset 1, modest chemical shift perturbation of a resonance upon addition of 0.5 equivalents $Dreb2a_{f.l.}$ which was undetectable at higher ligand concentrations. Inset 2, example of a cross-peak decreasing in intensity upon addition of $Dreb2a_{f.l.}$ (bottom left) which might indicate slow exchange and an unaffected cross-peak (upper right).
(EPS)

Figure S3   Sequence alignment of the *A. thaliana* and human Med25-ACID. Asterisks indicate identical amino acids. Secondary structure content of human Med25-ACID extracted from PDB ID 2XNF and secondary structure prediction for *A. thaliana* Med25-ACID using Jpred 3 server. Alpha helical content is highlighted in pink (H) and β-strands are highlighted in blue (B). Human Med25-ACID contains 7-strands and 3 α-helices while *A. thaliana* Med25-ACID is predicted to contain 7-strands and 2 α-helices.
(EPS)

Author Contributions

Conceived and designed the experiments: XA JB KB AO JS SB. Performed the experiments: XA JB KB. Analyzed the data: XA KB AO JS SB. Contributed reagents/materials/analysis tools: XA JB KB AO JS SB. Wrote the paper: XA JS SB.

References

1. Boube M, Joulia L, Cribbs DL, Bourbon HM (2002) Evidence for a mediator of RNA polymerase II transcriptional regulation conserved from yeast to man. Cell 110: 143–151.

2. Bourbon HM, Aguilera A, Ansari AZ, Asturias FJ, Berk AJ, et al. (2004) A unified nomenclature for protein subunits of mediator complexes linking transcriptional regulators to RNA polymerase II. Mol Cell 14: 553–557.

3. Kim YJ, Bjorklund S, Li Y, Sayre MH, Kornberg RD (1994) A multiprotein mediator of transcriptional activation and its interaction with the C-terminal repeat domain of RNA polymerase II. Cell 77: 599–608.

4. Hampsey M (1998) Molecular genetics of the RNA polymerase II general transcriptional machinery. Microbiol Mol Biol Rev 62: 465–503.

5. Holstege FC, Jennings EG, Wyrick JJ, Lee TI, Hengartner CJ, et al. (1998) Dissecting the regulatory circuitry of a eukaryotic genome. Cell 95: 717–728.

6. Fuxreiter M, Tompa P, Simon I, Uversky VN, Hansen JC, et al. (2008) Malleable machines take shape in eukaryotic transcriptional regulation. Nat Chem Biol 4: 728–737.

7. Toth-Petroczy A, Oldfield CJ, Simon I, Takagi Y, Dunker AK, et al. (2008) Malleable machines in transcription regulation: the mediator complex. PLoS Comput Biol 4: e1000243.

8. Meyer KD, Lin SC, Bernecky C, Gao Y, Taatjes DJ (2010) p53 activates transcription by directing structural shifts in Mediator. Nat Struct Mol Biol 17: 753–760.

9. Taatjes DJ, Naar AM, Andel F 3rd, Nogales E, Tjian R (2002) Structure, function, and activator-induced conformations of the CRSP coactivator. Science 295: 1058–1062.

10. Taatjes DJ, Schneider-Poetsch T, Tjian R (2004) Distinct conformational states of nuclear receptor-bound CRSP-Med complexes. Nat Struct Mol Biol 11: 664–671.

11. Bourbon HM (2008) Comparative genomics supports a deep evolutionary origin for the large, four-module transcriptional mediator complex. Nucleic Acids Res 36: 3993–4008.

12. Backstrom S, Elfving N, Nilsson R, Wingsle G, Bjorklund S (2007) Purification of a plant mediator from Arabidopsis thaliana identifies PFT1 as the Med25 subunit. Mol Cell 26: 717-729.

13. D'Alessio JA, Wright KJ, Tjian R (2009) Shifting players and paradigms in cell-specific transcription. Mol Cell 36: 924–931.

14. Levine M, Tjian R (2003) Transcription regulation and animal diversity. Nature 424: 147–151.

15. Mathur S, Vyas S, Kapoor S, Tyagi AK (2011) The Mediator complex in plants: structure, phylogeny, and expression profiling of representative genes in a dicot (Arabidopsis) and a monocot (rice) during reproduction and abiotic stress. Plant Physiol 157: 1609–1627.

16. Han EH, Rha GB, Chi YI (2012) MED25 is a mediator component of HNF4alpha-driven transcription leading to insulin secretion in pancreatic beta-cells. PLoS One 7: e44007.

17. Lee HK, Park UH, Kim EJ, Um SJ (2007) MED25 is distinct from TRAP220/MED1 in cooperating with CBP for retinoid receptor activation. EMBO J 26: 3545–3557.

18. Sela D, Conkright JJ, Chen L, Gilmore J, Washburn MP, et al. (2013) Role for human mediator subunit MED25 in recruitment of mediator to promoters by endoplasmic reticulum stress-responsive transcription factor ATF6alpha. J Biol Chem 288: 26179–26187.

19. Verger A, Baert JL, Verreman K, Dewitte F, Ferreira E, et al. (2013) The Mediator complex subunit MED25 is targeted by the N-terminal transactivation domain of the PEA3 group members. Nucleic Acids Res 41: 4847–4859.

20. Mittler G, Stuhler T, Santolin L, Uhlmann T, Kremmer E, et al. (2003) A novel docking site on Mediator is critical for activation by VP16 in mammalian cells. EMBO J 22: 6494–6504.

21. Yamamoto S, Eletsky A, Szyperski T, Hay J, Ruyechan WT (2009) Analysis of the varicella-zoster virus IE62 N-terminal acidic transactivating domain and its interaction with the human mediator complex. J Virol 83: 6300–6305.

22. Yang F, DeBeaumont R, Zhou S, Naar AM (2004) The activator-recruited cofactor/Mediator coactivator subunit ARC92 is a functionally important target of the VP16 transcriptional activator. Proc Natl Acad Sci U S A 101: 2339–2344.

23. Yang M, Hay J, Ruyechan WT (2008) Varicella-zoster virus IE62 protein utilizes the human mediator complex in promoter activation. J Virol 82: 12154–12163.

24. Bontems F, Verger A, Dewitte F, Lens Z, Baert JL, et al. (2011) NMR structure of the human Mediator MED25 ACID domain. J Struct Biol 174: 245–251.

25. Eletsky A, Ruyechan WT, Xiao R, Acton TB, Montelione GT, et al. (2011) Solution NMR structure of MED25(391-543) comprising the activator-interacting domain (ACID) of human mediator subunit 25. J Struct Funct Genomics 12: 159–166.

26. Klemm RD, Goodrich JA, Zhou S, Tjian R (1995) Molecular cloning and expression of the 32-kDa subunit of human TFIID reveals interactions with VP16 and TFIIB that mediate transcriptional activation. Proc Natl Acad Sci U S A 92: 5788–5792.

27. Kobayashi N, Boyer TG, Berk AJ (1995) A class of activation domains interacts directly with TFIIA and stimulates TFIIA-TFIID-promoter complex assembly. Mol Cell Biol 15: 6465–6473.

28. Lin YS, Ha I, Maldonado E, Reinberg D, Green MR (1991) Binding of general transcription factor TFIIB to an acidic activating region. Nature 353: 569–571.

29. Stringer KF, Ingles CJ, Greenblatt J (1990) Direct and selective binding of an acidic transcriptional activation domain to the TATA-box factor TFIID. Nature 345: 783–786.

30. Uesugi M, Nyanguile O, Lu H, Levine AJ, Verdine GL (1997) Induced alpha helix in the VP16 activation domain upon binding to a human TAF. Science 277: 1310–1313.

31. Xiao H, Pearson A, Coulombe B, Truant R, Zhang S, et al. (1994) Binding of basal transcription factor TFIIH to the acidic activation domains of VP16 and p53. Mol Cell Biol 14: 7013–7024.

32. Zhu H, Joliot V, Prywes R (1994) Role of transcription factor TFIIF in serum response factor-activated transcription. J Biol Chem 269: 3489–3497.

33. Park JM, Kim HS, Han SJ, Hwang MS, Lee YC, Kim YJ (2000) In vivo requirement of activator-specific binding targets of mediator. Mol Cell Biol 20: 8709–8719.

34. Ito M, Yuan CX, Malik S, Gu W, Fondell JD, Yamamura S, Fu ZY, Zhang X, Qin J, Roeder RG (1999) Identity between TRAP and SMCC complexes indicates novel pathways for the function of nuclear receptors and diverse mammalian activators. Mol Cell 3: 361–370.

35. Ikeda K, Stuehler T, Meisterernst M (2002) The H1 and H2 regions of the activation domain of herpes simplex virion protein 16 stimulate transcription through distinct molecular mechanisms. Genes Cells 7: 49–58.

36. Vojnic E, Mourao A, Seizl M, Simon B, Wenzeck L, et al. (2011) Structure and VP16 binding of the Mediator Med25 activator interaction domain. Nat Struct Mol Biol 18: 404–409.

37. Jonker HR, Wechselberger RW, Boelens R, Folkers GE, Kaptein R (2005) Structural properties of the promiscuous VP16 activation domain. Biochemistry 44: 827–839.

38. Langlois C, Mas C, Di Lello P, Jenkins LM, Legault P, et al. (2008) NMR structure of the complex between the Tfb1 subunit of TFIIH and the activation domain of VP16: structural similarities between VP16 and p53. J Am Chem Soc 130: 10596–10604.

39. McEwan IJ, Dahlman-Wright K, Ford J, Wright AP (1996) Functional interaction of the c-Myc transactivation domain with the TATA binding protein: evidence for an induced fit model of transactivation domain folding. Biochemistry 35: 9584–9593.

40. Shen F, Triezenberg SJ, Hensley P, Porter D, Knutson JR (1996) Transcriptional activation domain of the herpesvirus protein VP16 becomes conformationally constrained upon interaction with basal transcription factors. J Biol Chem 271: 4827–4837.

41. Sandholzer J, Hoeth M, Piskacek M, Mayer H, de Martin R (2007) A novel 9-amino-acid transactivation domain in the C-terminal part of Sox18. Biochem Biophys Res Commun 360: 370–374.

42. Choi Y, Asada S, Uesugi M (2000) Divergent hTAFII31-binding motifs hidden in activation domains. J Biol Chem 275: 15912–15916.

43. Aukerman MJ, Hirschfeld M, Wester L, Weaver M, Clack T, et al. (1997) A deletion in the PHYD gene of the Arabidopsis Wassilewskija ecotype defines a role for phytochrome D in red/far-red light sensing. Plant Cell 9: 1317–1326.

44. Cerdan PD, Chory J (2003) Regulation of flowering time by light quality. Nature 423: 881–885.

45. Devlin PF, Patel SR, Whitelam GC (1998) Phytochrome E influences internode elongation and flowering time in Arabidopsis. Plant Cell 10: 1479–1487.

46. Elfving N, Davoine C, Benlloch R, Blomberg J, Brannstrom K, et al. (2011) The Arabidopsis thaliana Med25 mediator subunit integrates environmental cues to control plant development. Proc Natl Acad Sci U S A 108: 8245–8250.

47. Kidd BN, Edgar CI, Kumar KK, Aitken EA, Schenk PM, et al. (2009) The mediator complex subunit PFT1 is a key regulator of jasmonate-dependent defense in Arabidopsis. Plant Cell 21: 2237–2252.

48. Fujita Y, Fujita M, Shinozaki K, Yamaguchi-Shinozaki K (2011) ABA-mediated transcriptional regulation in response to osmotic stress in plants. J Plant Res 124: 509–525.

49. Liu Q, Kasuga M, Sakuma Y, Abe H, Miura S, et al. (1998) Two transcription factors, DREB1 and DREB2, with an EREBP/AP2 DNA binding domain separate two cellular signal transduction pathways in drought- and low-temperature-responsive gene expression, respectively, in Arabidopsis. Plant Cell 10: 1391–1406.

50. Sakuma Y, Maruyama K, Osakabe Y, Qin F, Seki M, et al. (2006) Functional analysis of an Arabidopsis transcription factor, DREB2A, involved in drought-responsive gene expression. Plant Cell 18: 1292–1309.

51. Sakuma Y, Maruyama K, Qin F, Osakabe Y, Shinozaki K, et al. (2006) Dual function of an Arabidopsis transcription factor DREB2A in water-stress-responsive and heat-stress-responsive gene expression. Proc Natl Acad Sci U S A 103: 18822–18827.

52. Blomberg J, Aguilar X, Brannstrom K, Rautio L, Olofsson A, et al. (2012) Interactions between DNA, transcriptional regulator Dreb2a and the Med25 mediator subunit from Arabidopsis thaliana involve conformational changes. Nucleic Acids Res 40: 5938–5950.

53. Ohme-Takagi M, Shinshi H (1995) Ethylene-inducible DNA binding proteins that interact with an ethylene-responsive element. Plant Cell 7: 173–182.

54. Richardt S, Timmerhaus G, Lang D, Qudeimat E, Correa LG, et al. (2010) Microarray analysis of the moss Physcomitrella patens reveals evolutionarily conserved transcriptional regulation of salt stress and abscisic acid signalling. Plant Mol Biol 72: 27–45.

55. Riechmann JL, Meyerowitz EM (1998) The AP2/EREBP family of plant transcription factors. Biol Chem 379: 633–646.

56. Milbradt AG, Kulkarni M, Yi T, Takeuchi K, Sun ZY, et al. (2011) Structure of the VP16 transactivator target in the Mediator. Nat Struct Mol Biol 18: 410–415.

57. Ziarek JJ, Peterson FC, Lytle BL, Volkman BF (2011) Binding site identification and structure determination of protein-ligand complexes by NMR a semiautomated approach. Methods Enzymol 493: 241–275.

58. Schumann FH, Riepl H, Maurer T, Gronwald W, Neidig KP, et al. (2007) Combined chemical shift changes and amino acid specific chemical shift mapping of protein-protein interactions. J Biomol NMR 39: 275–289.

59. Dahlman-Wright K, Baumann H, McEwan IJ, Almlof T, Wright AP, et al. (1995) Structural characterization of a minimal functional transactivation domain from the human glucocorticoid receptor. Proc Natl Acad Sci U S A 92: 1699–1703.

60. Di Lello P, Jenkins LM, Jones TN, Nguyen BD, Hara T, et al. (2006) Structure of the Tfb1/p53 complex: Insights into the interaction between the p62/Tfb1 subunit of TFIIH and the activation domain of p53. Mol Cell 22: 731–740.

61. Wright PE, Dyson HJ (2009) Linking folding and binding. Curr Opin Struct Biol 19: 31–38.

62. Gohlke H, Kiel C, Case DA (2003) Insights into protein-protein binding by binding free energy calculation and free energy decomposition for the Ras-Raf and Ras-RalGDS complexes. J Mol Biol 330: 891–913.

63. Choi HJ, Huber AH, Weis WI (2006) Thermodynamics of beta-catenin-ligand interactions: the roles of the N- and C-terminal tails in modulating binding affinity. J Biol Chem 281: 1027-1038.

64. Akke M (2012) Conformational dynamics and thermodynamics of protein-ligand binding studied by NMR relaxation. Biochem Soc Trans 40: 419–423.

65. Janin J, Bahadur RP, Chakrabarti P (2008) Protein-protein interaction and quaternary structure. Q Rev Biophys 41: 133–180.

66. Kastritis PL, Bonvin AM (2013) On the binding affinity of macromolecular interactions: daring to ask why proteins interact. J R Soc Interface 10: 20120835.

67. Mills JL, Liu G, Skerra A, Szyperski T (2009) NMR structure and dynamics of the engineered fluorescein-binding lipocalin FluA reveal rigidification of beta-barrel and variable loops upon enthalpy-driven ligand binding. Biochemistry 48: 7411–7419.

68. Piskacek S, Gregor M, Nemethova M, Grabner M, Kovarik P, et al. (2007) Nine-amino-acid transactivation domain: establishment and prediction utilities. Genomics 89: 756–768.

69. Uesugi M, Verdine GL (1999) The alpha-helical FXXPhiPhi motif in p53: TAF interaction and discrimination by MDM2. Proc Natl Acad Sci U S A 96: 14801–14806.